Method for detecting and characterising actinide-bearing micro-particles in soils and sediment of the Fukushima Prefecture, Japan

Hugo Jaegler, Fabien Pointurier, Yuichi Onda, Jaime Angulo, Nina Griffiths, Agnès Moureau, Anne-Laure Faure, Olivier Marie, Amélie Hubert, O. Evrard

HAL Id: cea-02615745

https://cea.hal.science/cea-02615745

Submitted on 25 May 2020

1 # A methodology for detecting and characterising actinide-bearing micro-
2 particles in soils and sediment of the Fukushima Prefecture, Japan

3

4 Hugo Jaegler[1], Fabien Pointurier[2], Yuichi Onda[3], Jaime F. Angulo[4], Nina M. Griffiths[4], Agnes

5 Moureau[4], Anne-Laure Faure[2], Olivier Marie[2], Amélie Hubert[2] & Olivier Evrard[1]*

6

7 [1]Laboratoire des Sciences du Climat et de l'Environnement, LSCE/IPSL, Unité Mixte de

8 Recherche 8212 (CEA-CNRS-UVSQ), Université Paris-Saclay, F-91198 Gif-sur-Yvette, France

9 [2]CEA, DAM, DIF, F-91297 Arpajon, France

10 [3]Center for Research in Isotopes and Environmental Dynamics (CRIED), University of Tsukuba,

11 Tsukuba, Japan

12 [4]Laboratoire de Radio Toxicologie, CEA, Université Paris-Saclay, 91297 Bruyères-le-Châtel,

13 France

14

15 (*) Corresponding author (email address: olivier.evrard@lsce.ipsl.fr).

16

Abstract:

18 The Fukushima Dai-ichi Nuclear Power Plant (FDNPP) accident released limited amounts of

19 actinides on soils of Japan. Characterisation of these particles is essential to determine the fate

20 of actinides in the environment. The method presented in this paper, based on α-tracks

21 detections, microscope observations and mass-spectrometry measurements, was designed to

22 identify and characterize actinide-bearing particles in soil samples. The method was tested on a

23 road dust sample collected in the main radioactive plume of the Fukushima region. Accordingly,

24 α-tracks detection was demonstrated to provide a powerful technique to localise these particles

25 and prepare their morphological, elemental and isotopic characterization.

26

27 ## Keywords

28 Fukushima Dai-ichi Nuclear Power Plant accident; actinide-bearing particles; Solid State Nuclear

29 Track Detector; microscope characterisation; mass spectrometry

30

31 ## Introduction

32 Most radionuclides released into the environment during the Fukushima Dai-ichi Nuclear Power

33 Plant (FDNPP) accident were activation or fission products, like radioiodine or radiocesium. In

34 contrast, the estimated releases of uranium and plutonium emitted in the atmosphere were

35 comparatively very low [1]. Therefore, only trace amounts of plutonium [2–4] and uranium [1,

36 5–8] isotopes from the nuclear fuel have been detected in environmental samples collected in

37 the vicinity of the power plant.

38

39 It has been shown that actinides released by nuclear events like atmospheric tests [9], nuclear

40 weapon accidents [10, 11] and more recently the Chernobyl accident [12] are at least in part

41 contained in microparticles. After the FDNPP accident, several authors investigated the

42 occurrence of radioactive microparticles, and successfully detected cesium-rich microparticles in

43 the environment [13–15]. These microparticles were identified from ^{137}Cs gamma emission

44 using gamma-imaging plates. However, when detected, uranium was a minor constituent of

45   these particles [16–18]. Actinide-bearing microparticles do not necessarily contain fission

46   products, because actinide and fission products are characterised by different levels of volatility

47   and melting points. Actinide-bearing particles therefore are not necessarily detectable with

48   gamma-radiography. Following the FDNPP accident release of plutonium particles was

49   suspected [19, 20] and the emission of uranium particles was confirmed [16, 21]. The post-

50   accidental fate of these actinides is strongly influenced by several factors including the size, the

51   geometry, the microstructure and the different elemental (i.e. in other chemical elements than

52   actinides) and molecular composition of these particles. These characteristics require

53   investigation as they will influence the dissolution, the mobilization, the transport or the

54   retention processes affecting the actinides [9].

55

56   Since uranium and plutonium were already present in the environment before the FDNPP

57   accident, as a result of the global fallout associated with atmospheric nuclear weapon tests, the

58   source of these actinides need to be carefully investigated [22]. Furthermore, compared with

59   the very low additional input of FDNPP-derived uranium, naturally-occurring uranium is found at

60   concentrations ranging around 1.9 ± 1.2 µg/g , 2σ in the Japanese soils ([23, 24]). These sources

61   of uranium are characterised by different isotopic compositions, mainly for ^{235}U and ^{238}U.

62   Moreover, the measurement of ^{236}U – a minor uranium isotope - may also provide a strong

63   indicator of the anthropogenic source of uranium [1, 25], as the $^{236}U/^{238}U$ isotope ratio provides

64   a very good discrimination between different sources of uranium [6]. Measurements of these

65   isotope ratios were mainly performed by "bulk" analyses [1, 5–8]. The characterisation of

66   FDNPP-derived uranium particles deserves isotopic analyses atthe particle scale.

67

68   To the best of our knowledge, Imoto et al. [15] are the only authors who determined uranium

69   isotope ratios based on Secondary Ion Mass Spectrometry (SIMS) measurements in three

70   caesium-containingmicroparticles extracted from paddy soil and gravel located below

71   drainpipes from the Fukushima region. They identified the source of uranium in these particles

72   showing an isotopic ratio ^{235}U/^{238}U value close to 0.03 ± 0.003 (compared to 0.0072 in natural

73   uranium), which is characteristic of enriched nuclear fuel. They thereby demonstrated that

74   these particles were composed of uranium from FDNPP. However, these particles were

75   detected with gamma-imaging plates, which does not allow the detection of particles with

76   uranium as a major component. To do so, nuclear track radiography provides a more

77   appropriate screening method to identify selectively uranium particles, when analysing a soil

78   sample or another type of powder sample composed of large amounts of any type of particles.

79

80   Nuclear track radiography has been used in numerous studies [26, 27], mainly in those

81   investigations conducted after the Chernobyl accident [9, 28–30], to identify and extract "hot"

82   radioactive particles from soil samples. These experiments consist in positioning a contaminated

83   sample in close contact with a Solid State Nuclear Track Detector (SSNTD). When emitted by

84   radionuclides contained in the particles, α-particles generate damage on the SSNTD located just

85   above the particle, leaving characteristic tracks (the so-called α-tracks) with well-known star-

86   shapes whose centre is located just above the α-emitting particle.

87

88   The current research was conducted on a road dust sample, also referred to as "black

89   substance", in order to maximize the probability to detect anthropogenic particles. Indeed, after

90   the FDNPP accident, several studies [1, 8] were performed on this type of material, which is

91   composed of aerosol and tyre particles, asphalt and environmental residues including soil and

92   lichen debris. "Black substances" are accumulated on the sides of the roads as a result of wind

93   and water erosion, and were shown to contain particularly high concentrations of radionuclides.

94   In previous studies [1, 8], this type of material was analysed using "bulk" analytical methods to

95   characterise uranium and plutonium isotope ratios, i.e. without focusing the investigations on

96   individual actinide-bearing micro particles.

97

98   To meet this goal a preliminary study was carried out in order to check the occurrence of μm-

99   sized actinide-bearing particles in a powder sample. Then, we developed a new methodology

100 for the detection and isolation of these particles.The elemental, morphological and isotopic

101 characterisation of these particles was finally performed together with the isotope analyses on

102 these μm-sized particles. The overall objective of this work was therefore to develop an

103 innovative method for the detection and characterisiation of actinide-bearing micro-particles

104 found in environmental samples contaminated with the radioactive fallout associated with the

105 FDNPP accident.
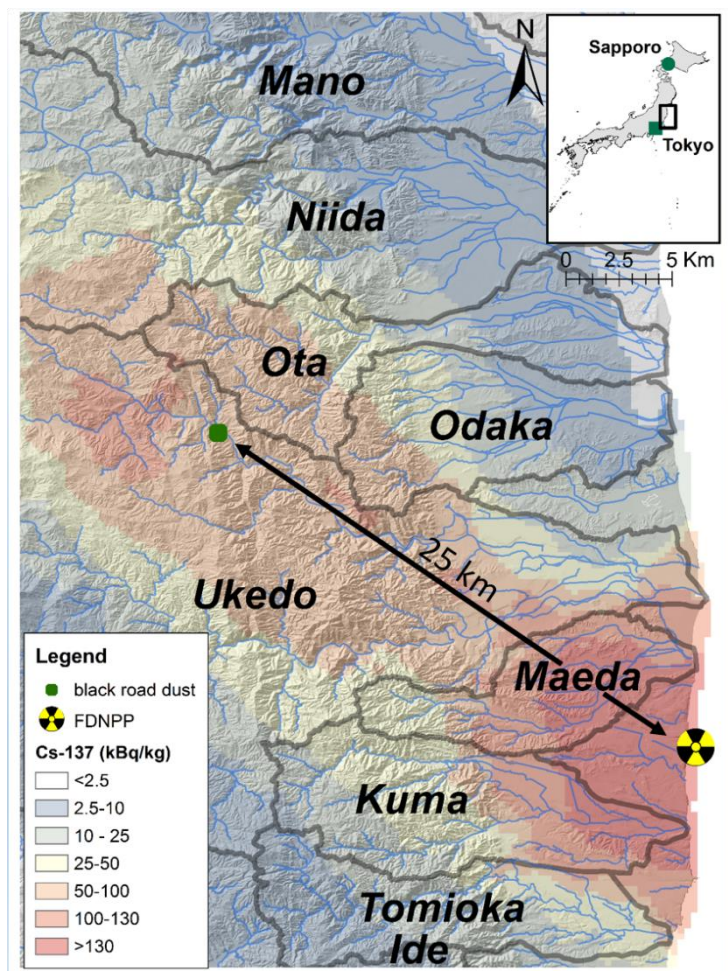
106

107 ## Methodology

108

109   Sampling

110

111   The "black substance" sample was collected in November 2015 in the Ukedo River catchment

112   along a road located in the main radioactive plume, approximately 25 km to the northwest of

113   FDNPP (GPS coordinates: N 37.553371; E 140.834940, see Fig. 1) in the Namie Municipality. The

114   emitted radiation dose measured at the sampling location with a radiameter (LB123 D-H10,

115   Berthold Technologies) exceeded 100 µSv h^{-1} at 1-cm distance from the soil surface.

116

118   **Fig. 1** Location of the sampling site of the road dust sample within the main radioactive pollution plume of

119   Fukushima, Japan

120

121 Preliminary study: sample screening by means of Scanning Electron Microscopy and Energy-

122 Dispersive X-ray spectrometry

123

124 The goal of this preliminary study was to check the presence of actinide particle in sub-samples,

125 so as to confirm that the collected sample was appropriate for the implementation of the

126 developed methodology. For this purpose, samples were directly analysed by Scanning Electron

127 Microscopy (SEM) and Energy-Dispersive X-ray spectrometry (EDX). Observations by SEM (FEI

128 Quanta 3D FEG, Eindhoven, The Netherlands) were conducted in the low vacuum mode (60 Pa)

129 to allow the analysis of non-conductive materials, with the use of backscattered electron

130 detectors on a wide field (approximately 500 µm by 500 µm). This allows the detection of the

131 particles with a density higher than an average atomic number of 20 with the chosen analytical

132 parameters (detection size limit is 0.55 µm for uranium particles), which likely corresponds to

133 radioactive particles. Among the detected particles, only those identified as "uranium particles"

134 (i.e. those for which uranium was the major constituent) were analysed individually by EDX

135 spectroscopy (EDAX Apollo SDD 10 mm^2) for chemical characterisation. Due to the low

136 abundance of plutonium in nuclear fuel (both irradiated UO_2 and MOX) compared to that of

137 uranium, it is very unlikely to detect directly plutonium in particles. Accordingly, only those

138 particles in which uranium is a major constituent were initially targeted by these experiments.

139

140 In this preliminary experiment, two milligrams of the sample were randomly collected with

141 Sticky Carbon Tapes (SCT, n=14) dabbed onto walls of the vials containing the road dust sample.

142 SCTs consist of double sided carbon-based electrically conductive and non-porous adhesive

143 mounted on an aluminum holder, which is a suitable support for SEM and EDX analyses.

144 Accordingly, SCTs were directly analysed by SEM and EDX following a three-step process: i)

145 automated search for particles with high average atomic numbers, including particles for which

146 uranium is the major constituent, using the Gun Shot Residue (GSR) software. This software also

147 provides an EDX spectrum and indicates the major elemental constituents of the detected

148 particles; ii) more precise EDX spectrum for each particle identified as 'uranium-particle' with a

149 longer acquisition time (one minute instead of a few seconds) to confirm the presence of

150 uranium as a major constituent and to identify minor constituents (i.e. with concentrations

151 above ~1%); iii) high resolution imaging of the detected actinide particles with high

152 magnification.

153

154 In previous studies, uranium was shown to be associated with Zn-Fe oxide [15] or trapped in

155 spherical SiO_2 particles [14], so that the occurrence of particles of Fe and Zn or spherical

156 particles of Si were also investigated in order to verify the possible presence of uranium and Cs

157 as minor constituents in these particles.

158

159 Nuclear track autoradiography to isolate actinide-bearing particles

160

161 Following investigation of the occurrence of actinide-bearing particles in the sample, the

162 difficulty of micro-particle transfer from the SCTs to carbon plate to conduct isotopic

163 measurements led to the development of a second screening method. To this end, the

164 detection and the isolation of actinide-bearing particles were performed through alpha-

165 autoradiography using a Solid-State Nuclear Track Detector (SSNTD).

166

167 The SSNTD used in the current study was the Tastrak™ detector (TASL, Ltd, Bristol, UK) with a

168 density of 1.30 g/cm^3, a thickness of 500 μm and a cut-off angle of 20° for alpha particles. A key

169 point for α-track autoradiography is the measurement of the yield of the experiments, as it

170 determines the capability of the SSNTD to record the activity of particles. We experimentally

171 estimated the yield through by the deposition of different concentrations of a ^{242}Pu solution

172 (Plutonium-242 Radioactivity Standard, Standard Reference Material 4334I, National Institute of

173 Standards & Technology, CERCA-LEA, F 26701 PIERRELATE cedex; www.lea-cerca.com) on a

174 rough filter to simulate the particulate nature of the sample. The SSNTD was put in close contact

175 with the filter that was protected by mylar foil (3.5 μm thickness) during 6, 10 and 11 weeks.

176 Thenumbers of α-tracks on the SSNTD were counted by microscopy observation using a ccd

177 camera piloted by Archimed (version 7.0.10) and the number of tracks quantified using Histolab

178 (version 8.0.10) form Microvision instruments, (Lisses, France; https://www.microvision.fr). The

179 number of tracks allowed to calculate the activity and to compared it with the activity of the

180 strandard reference solution. The experimental yield cannot exceed 50 %, as only half of the α-

181 particles are emitted upwards and will therefore impact the SSNTD. Moreover, alpha-particles

182 are subject to self-attenuation within the particle and in the bulk sample, which will significantly

183 reduce the yield factor. We estimated the yield of the α-track experiments to be 30 % of the

184 ^{242}Pu certified solution. Accordingly, the yield correction factor (η) was set to 0.3 in the

185 calculations. This value is in good agreement with those found in the literature [26].

186

187 With regard to the road dust sample, a thin sample layer of dust was deposited on square

188 polycarbonate support plates (n = 90) with collodion to ensure a perfect immobilisation of the

189 sample during experiments. Sample support plates and SSNTD were welded and pierced

190 together in order to provide coordinates in order to locate of α-emitting particles for isolation.

191 Tastrak SSTND was positioned in close contact with the sample during 2, 4 and 6 months.

192 Twenty SSNTD plates were revealed and observed after 2 months, then twenty additional plates

193 after 4 months and, finally, fifty plates after 6 months. At the end of each experiment, SSNTD

194 was etched in a 6 M NaOH solution at 80°C during 1 h.   Tracks were observed by optical

195 microscopy. After localisation of α-track clusters, SSNTD and plates were separated and α-

196 emitting particles were localised using the coordinates on both SSNTD and plates. The support

197 plates containing the α-emitting particles were then analysed by SEM and EDX, using the same

198 methodology as described for the preliminary experiments (see section 'Sample screening by

199 means of SEM/EDX').

200

201 The number of α-tracks per cluster was used to estimate the activity of the corresponding

202 particle. It was hypothesized that: 1) all α-emitters had the same yield, 2) the samples were

203 assumed to be composed of the following three proportions of actinides:

204

205 • Composition 1: natural uranium ore with 99.3 % of ^{238}U, 0.720 % of ^{235}U and 0.005 % of

206 ^{234}U, which contains also α-emitter daughter nuclides of ^{235}U and ^{238}U - ^{234}U decay chains

207 (devoid of plutonium);

208   •   Composition 2: nuclear fuel composition at the moment of the accident in reactor 1 [31],

209   with 97.5 % of ^{238}U, 1.66 % of ^{235}U, 3.10×10^{-4} % of ^{234}U, 0.455 % of ^{239}Pu and 0.157 % of

210   ^{240}Pu ;

211   •   Composition 3: MOX fuel with 2.5 % of plutonium (80 % of ^{239}Pu and 20 % of ^{240}Pu) and

212   97.5 % of uranium (98 % of ^{238}U, 2 % of ^{235}U and 0.01 % of ^{234}U) (Reactor 3);

213   •   Composition 4: natural uranium with 99.3 % of ^{238}U, 0.720 % of ^{235}U and 0.005 % of ^{234}U,

214   which contains also α-emitting daughter radionuclides from ^{235}U and ^{238}U - ^{234}U decay

215   chains and global fallout plutonium (estimation of ^{239}Pu and ^{240}Pu abundances based on

216   the ^{239}Pu concentrations measured in Japan [32])

217

218 Then, the number of atoms of actinide in the particle (n_{act}) was estimated based on the number

219 of α-tracks recorded on the SSNTD ($n_{\alpha\text{-tracks}}$) divided by the yield η, the time t (in second), a_i the

220 atomic abundances of the α-emitter isotope i (which is an isotope of uranium or plutonium),

221 and the λ_i the decay constant of α-emitter i (which is an isotope of uranium or plutonium) as in

222 Eq. (1).

$$n_{act} = \frac{n_{\alpha\text{-tracks}}}{\eta \times \Delta t \times \sum_i (a_i \times \lambda_i)} \tag{1}$$

223

224 The equivalent diameter ϕ of the particle (assumed to be spherical and made of UO$_2$) is

225 therefore calculated as in Eq. (2) [33].

$$\phi = \sqrt[3]{\frac{6 \times n_{\alpha\text{-tracks}} \times M_{UO2}}{\pi \times \rho \times \mathcal{A} \times \eta \times \Delta t \times \sum_i (a_i \times \lambda_i)}} \tag{2}$$

226

227   Where $\mathcal{A}$ is the Avogadro Number, ρ the density of UO$_2$ (10.97 g/cm^3), M_{UO2} the molar mass of

228   UO$_2$ (270 g/mol).

229

230   Secondary Ion Mass Spectrometer measurements

231

232   SIMS measurements were performed to determine the isotopic composition of the particles.

233   Prior to SIMS analysis, a small part of the polycarbonate plate (square shape, 5 mm side) was

234   cut around the theoretical position of the uranium-bearing particle. These subsamples that

235   were assumed to include the particle were dissolved in ethanol overnight and deposited on a

236   carbon plate with PolyIsoButylen acting as a sticking agent. Samples were heated in a furnace at

237   400°C for 30 min to evaporate the liquid deposition and eliminate any organic residue.

238

239   Details on SIMS function have been described elsewhere [34]. In brief, the SIMS instrument is a

240   double focusing instrument (Cameca IMS 7f, Gennevilliers, France) equipped with a

241   duoplasmatron (O$_2^+$) source. This primary beam was accelerated to 15 keV, whereas the

242   secondary ion beam was acccelerated to 5 keV. The mass resolving power was set to 450 in

243   order to obtain flat-top peak. An Automatic Particle Measurement (APM) software allows the

244   efficient detection of uranium particles, through the acquisition of ion images of ^{238}U$^+$ in a series

245   of 500 μm × 500 μm fields over the entire carbon plate. Ion images at m/z=233 and 234 were

246   also recorded and used as indicators of isobaric interference levels in the sample. After APM

247   data acquisition, microbeam measurements were performed on the selected individual particle.

248   ^{234}U$^+$, ^{235}U$^+$, ^{236}U$^+$ and ^{238}U$^+$ isotopic intensities were measured to determine precisely the

249   uranium isotopic compositions. Mass bias of these measurements was corrected through the

250   measurement of certified particles, and the ^{236}U signal was corrected from ^{235}UH species. Ion

251   images of ^{235}U$^+$ and ^{238}U$^+$ were also acquired for visualizing the particle. In order to investigate

252   the potential presence of plutonium isotope in the particle, a mass scan was also performed
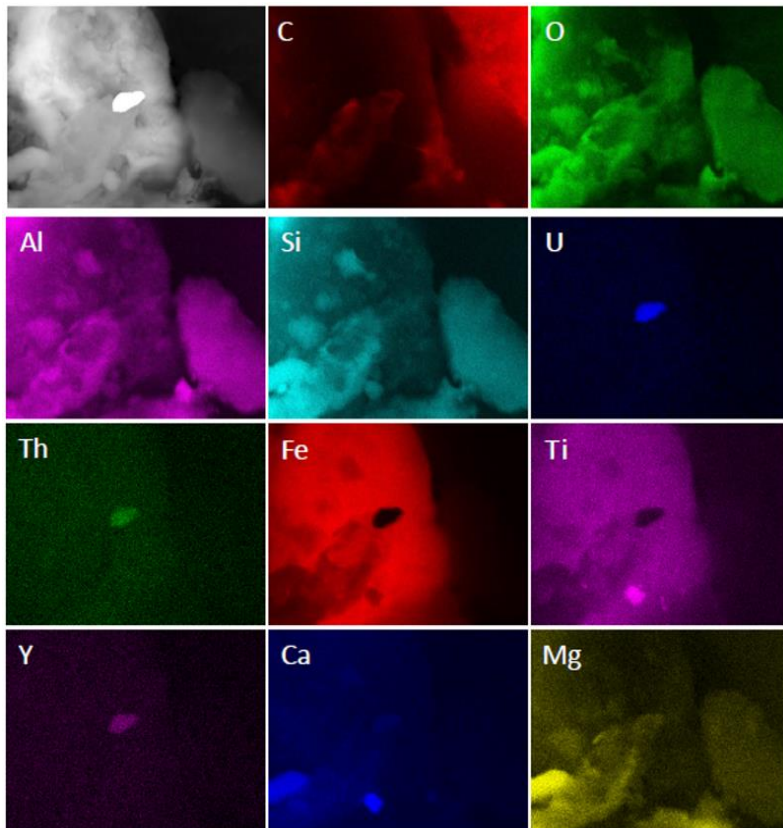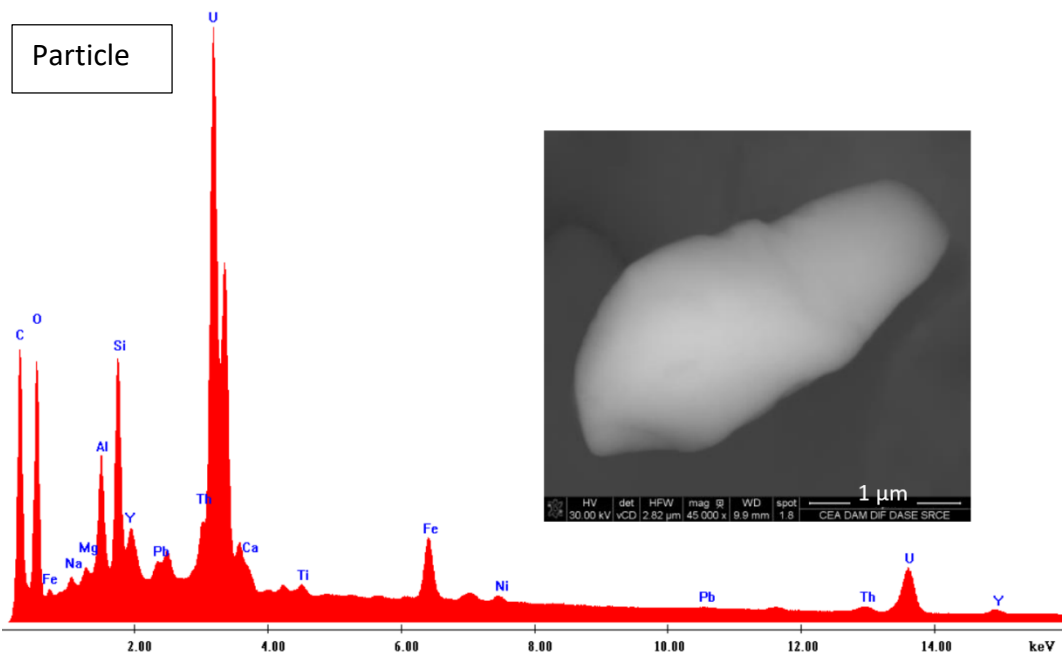
253   from ^{238}U to ^{242}Pu masses.

254

255   **Results and discussion**

256

257   Sample screening by means of SEM/EDX

258

259   Four uranium particles were detected by SEM from the 14 analysed SCTs used to collect sub-

260   samples of the road dust sample. Pictures of the particle 1 (photography, EDX spectra and

261   elemental mappings) are presented in Fig. 2; pictures of the 3 other particles are provided in

262   Supplementary Information (Fig. S1 – S3). The size of these particles ranged from 2 to 3 µm. In

263   addition to uranium, these particles mainly contained C, O, Al, Si, U and Fe. Traces of Na, Mg, Y,

264   Pb, Th, Ca, Ti, Co and Ni were also detected by EDX. However, no trace of Cs, Zn or Pu was

265   detected, with detection limits of ~1%.

266

267

268 **Fig. 2** Electronic image, EDX spectrum and elemental mapping of the particle #1 identified as an U-bearing particle.

269 The mapping shows qualitatively that some elements (C, O, Al, Si, Fe, Ti) detected in the EDX spectrum may come

270   from surrounding particles, whereas Y, Th, Ca and Mg are obviously present in the particle. This is an indication that

271   this U-bearing particule may be of natural origin

272

273   This preliminary study confirms the presence of uranium particles in the samples collected in

274   the vicinity of the FDNPP. Caesium and plutonium, if present are in very low amounts that

275   arebelow the EDX detection limits (approximately 1%). However, EDX analyses do not allow the

276   determination of the source of these uranium particles (FDNPP or naturally-occurring). Further

277   analyses, including isotopic measurements, were required to confirm the sources of these

278   particles. Unfortunately, the direct isotope analysis by SIMS on SCTs is not possible (because of

279   the melting of the conductive glue under the primary ion beam). Moreover, the micro-sampling

280   of particles, which would be required to deposit them on a support material suitable for SIMS

281   analysis (i.e. perfectly plane and conductive), is not possible on SCTs. Also, the automatic search

282   of particles by means of GSR software is very time-consuming and ineffective for analysis of

283   relatively large amounts of sample (at least a few mg). Accordingly, nuclear track

284   autoradiography experiments were performed to increase the quantity of analysed material and

285   to conduct both morphological and elemental analyses by SEM/EDX, and isotope analysis by

286   SIMS on the detected α-emitting particles.

287

288   Lastly, 9 FeZn particles were also analysed. Their sizes ranged from 3.5 μm to 20 μm. Their

289   shape was also heterogeneous: some particles were sharp and rough, while others were

290   completely spherical (see examples provided on Fig. S4). They were mainly composed of C, O,

291   Al, Si, Fe and Zn. Trace amounts of Na, Mg, P, S, K, Ca, Ti, Mn and Cu were also detected.

292   However, no trace of Cs, Pu and U could be detected in these particles.

293

294   It should be noted that many spherical Si particles were observed. Twenty of these were

295   analysed (one example is provided on Fig. S5). The size of these particles ranged from 4 to

296   10 μm, and they were mainly composed of C, O, Al and Si. Traces of C, O, Na, Mg, Al, Si, S, K, Ca,

297   Ti and Mn were also detected. Again, no trace of U, Pu and Cs could be detected in these

298   spherical Si particles.

299

300   α-track autoradiography experiments or Solid-State Nuclear track Detector experiments

301

302   Of the 90 prepared SSNTD plates, 20 were revealed after 2 months of exposure, 20 were

303   revealed after a 4-month exposure and the last 50 after a 6-month exposure. The total numbers

304   of detected particles for each exposure are given in Table 1.
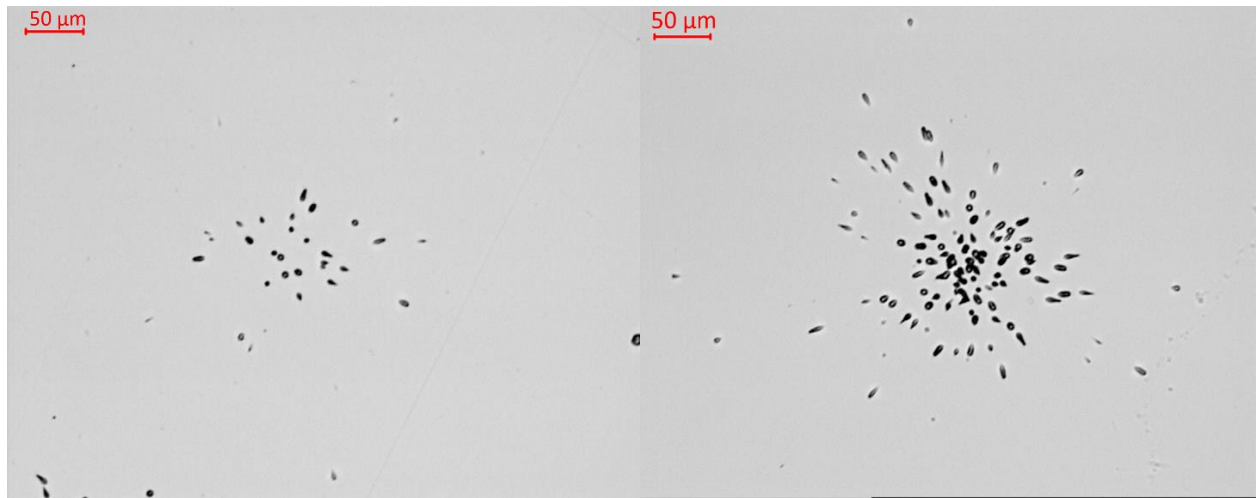
305

306   **Table 1** Summary of particle detection and analysis after α-track radiography.

Time of exposure	Number of revealed SSNTD plates	Number of detected particles	Number of particles analysed by SEM and EDX
2 months	20	27	3
4 months	20	30	9
6 months	50	40	16
TOTAL	90	97	28

307

308   However, most of these clusters have less than 20 α-tracks (Fig. 3, left). For example, the

309   number of detected particles after the 2-month exposure revealed that only 3 clusters were

16

310   composed of more than 100 α-tracks (Fig. 3, right), with 104 (particle A), 118 (particle B) and

311   162 (particle C) α-tracks recorded on the SSNTD, respectively.

312

313
314   **Fig. 3** Optical images of α-tracks clusters after 2 months of exposure. Left: example of a small cluster, with less than

315   20 α-tracks. Right: example of large cluster, with more than 100 α-tracks

316

317   The size of these particles can be roughly estimated (Table 2), through the comparison of

318   potential scenarios on the composition of the particles (see the Methodology section). These

319   theoretical calculations demonstrated that, for a given activity, particles are smaller by almost

320   one order of magnitude when they contain FDNPP-derived plutonium.

321

322

323

324

325

326 **Table 2** Theoretical particle sizes, based on the following hypotheses made on the composition of the particles: 1:

327 natural uranium; 2: FDNPP uranium fuel; 3: FDNPP MOX fuel ; 4 : natural uranium and global fallout plutonium (see

328 Methodology section). Particles A, B and C correspond to the three large clusters detected on the SSNTD after a

329 two-month exposure and analysed by SEM and EDX (see Table 1).

	Composition 1			Composition 2			Composition 3			Composition 4		
Particle	A	B	C	A	B	C	A	B	C	A	B	C
Number of α-tracks recorded	104	118	162	104	118	162	104	118	162	104	118	162
Theoretical equivalent diameter (μm)	3.9	4.1	4.5	0.82	0.85	0.95	0.53	0.55	0.61	3.9	4.1	4.6

330

331

332 After 4 months of exposure, 20 other SSNTD plates were revealed and observed. 30 α-tracks

333 clusters were observed, among which 9 were particularly dense in terms of number of α-tracks

334 recorded on the SSNTD. Finally, after 6 months of exposure, the last 50 SSNTD were revealed

335 and observed: 40 α-track clusters were detected, among which 16 were particularly dense. 28

336 particles corresponding to the more α-emitting clusters identified after the 2, 4 and 6-month

337 exposure times were then observed and analysed by SEM.
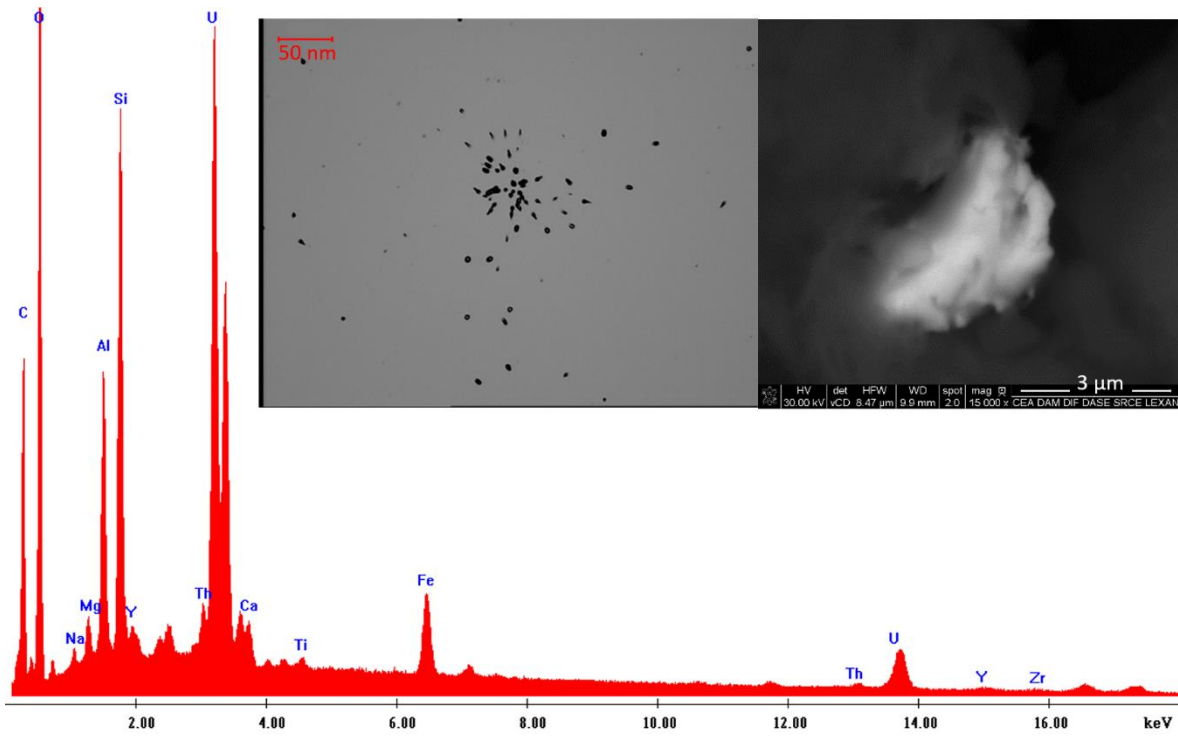
338

339 SEM observation of particles

340

341 Four types of particles were observed by SEM: 1) 10 zircon particles ($ZrSiO_4$) with sizes (apparent

342 mean diameter) ranging from 30 to 100 μm. It should be noted that α-tracks are produced by U

343 and Th isotopes that are substituted to Zr in zircon. 2) 7 particles of thorite, composed by

344   ThSiO$_4$, (mainly ^{232}Th, T$_{1/2}$ = 1.4×10^{10} y) of approximately 20 μm. 3) 7 Monazite particles

345   composed by (Ce, La, Nd, Pr)PO$_4$ with size ranging from 30 to 100 μm. Th is also present as a

346   minor constituent and detected by EDX in these particles. 4) 4 uranium particles were detected.

347   The size of these particles was estimated to approximately 4 μm for particle 1 (Fig. 4), 4 μm for

348   particle 2 (Fig. 5), 6 μm for particle 3 (Fig. 6) and 8 μm for particle 4 (Fig. 7). Th, Si, O, Fe, Al and

349   Y were also detected as minor constituents in the uranium particles. It should be noted that

350   presence of other chemical elements than uranium (Si, Fe, Al, etc.) may be due to intrinsic

351   impurities, and/or to the influence of neighbouring mineral particles which are partly included

352   in the analysed volume. In the first case, particles could be made of naturally-occurring uranium

353   or uranium from FDNPP mixed with concrete or other metals. However the presence of Th as a

354   minor constituent was detected in all four particles which provides a strong indicator for a

355   natural origin since Th is absent in the nuclear fuel but abundant in many uranium ores [35].
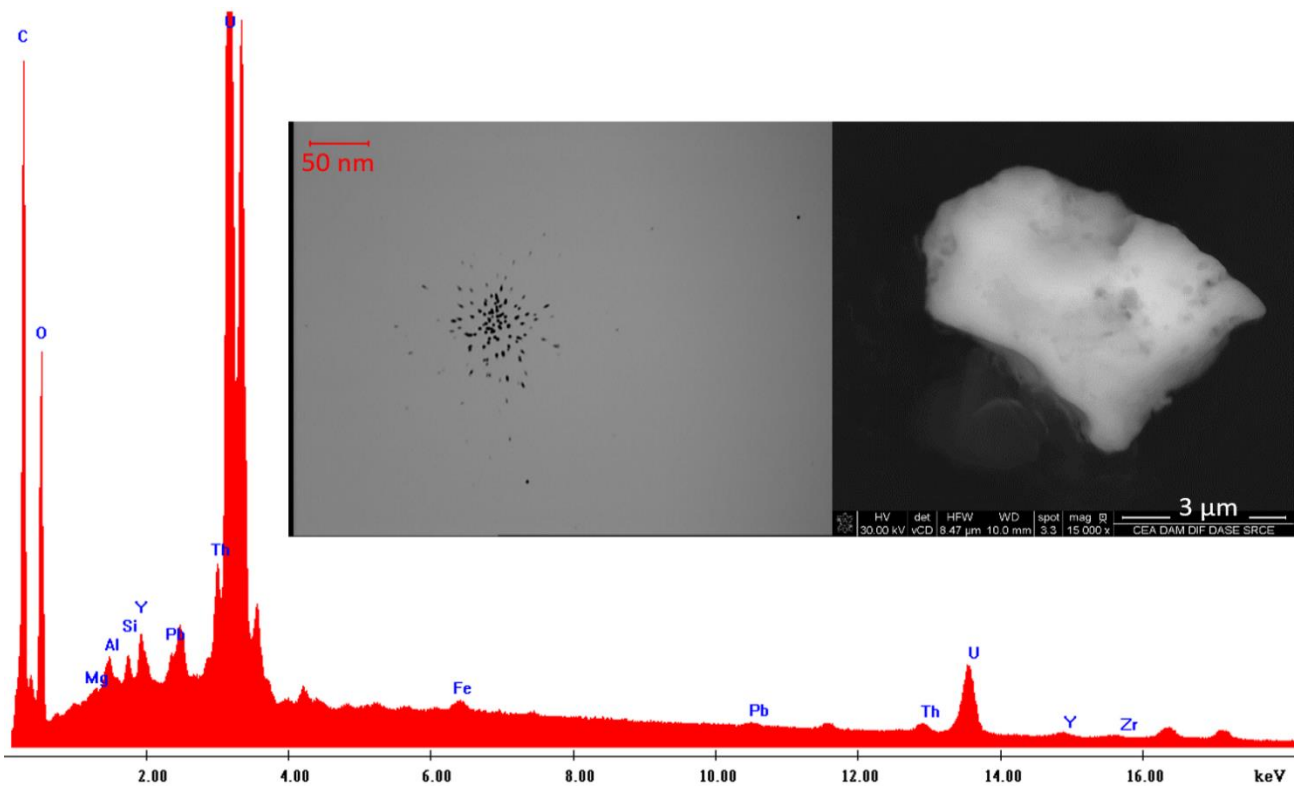
356

357

Fig. 4 Optical image of α-tracks recorded on the SSNTD after a 4 month-exposure time, SEM image and associated
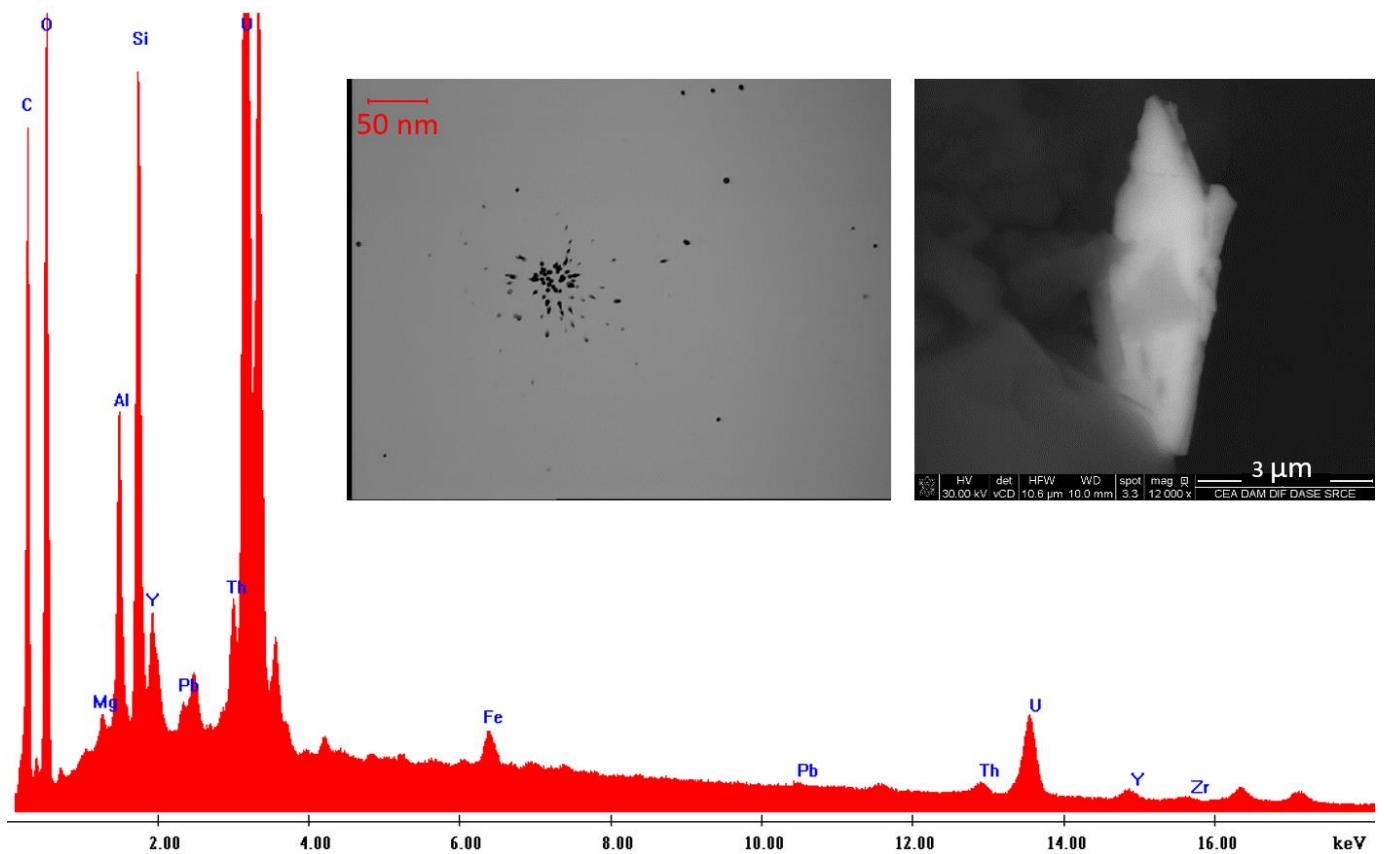
EDX spectrum for particle #1

360   **Fig. 5** Optical image of α-tracks recorded on the SSNTD after a 4 month-exposure time, SEM image and associated

361   EDX spectrum for particle #2

362 **Fig. 6** Optical image of α-tracks recorded on the SSNTD after a 6 month-exposure time, SEM image and associated

363 EDX spectrum for particle #3

364

365 **Fig. 7** Optical image of α-tracks recorded on the SSNTD after a 6 month-exposure time, SEM image and associated

366 EDX spectrum for particle #4

367

368 Composition and origin of uranium particles

369

370 With the activities calculated according to the α-tracks recorded on the SSNTD and based on the

371 yield previously determined (about 30 %), the size (equivalent diameter) of the uranium

372 particles can be estimated. The number of α-tracks recorded on the SSNTD and the calculated

373   equivalent diameters deduced according to the four hypothetical compositions considered in

374   this study are compiled in Table 3.

375

376   **Table 3** Theoretical particle sizes (equivalent diameters assuming UO_2 density) of the uranium particles localized by

377   means of α-track autoradiography and characterised by SEM/EDX according to the four hypothetical compositions
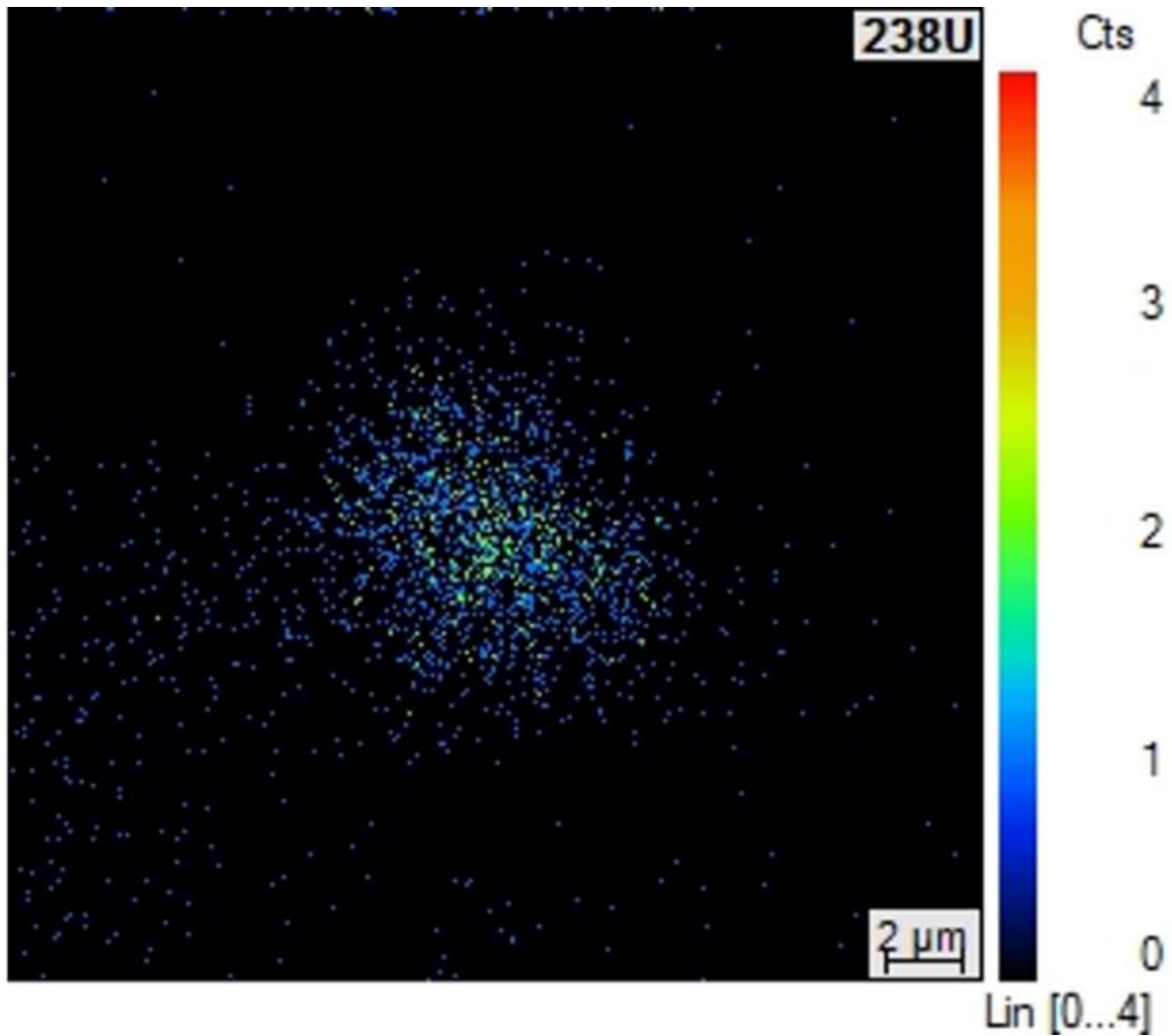
378   considered in this study.

Particle number		1	2	3	4
Exposure time (months)		4	4	6	6
Number of α-tracks recorded		98	53	117	76
Calculated equivalent diameter (µm)	composition 1	3.0	2.5	2.8	2.4
	Composition 2	0.64	0.52	0.59	0.51
	Composition 3	0.41	0.33	0.38	0.33
	Composition 4	3.0	2.5	2.8	2.4

379

380   Compared with the sizes estimated based on the SEM observations (4, 4, 6 and 8 µm,

381   respectively), the results suggest that these particles did not contain FDNPP-derived plutonium,

382   as their activities would be higher or the particles would be smaller. Accordingly, this first

383   estimation suggests that the U is of natural origin.

384

385   To investigate further this issue, SIMS measurements were performed on particle 1. Other

386   particles could not be recovered after collodion dissolution and sample deposition onto graphite

387   disks. After detection by APM, an ion image was acquired (Fig. 8). The isotopic composition was

388   determined to $^{235}U/^{238}U = 0.00736 \pm 0.00017$ and $^{234}U/^{238}U = (5.37 \pm 0.83) \times 10^{-5}$, after mass bias

389   correction. These results demonstrated unambiguously that this particle contained only natural

390   uranium. Nevertheless, plutonium isotopes were investigated through the scanning of the

391   particle from 239 to 242 atomic mass units. As expected, no plutonium isotope was detected in
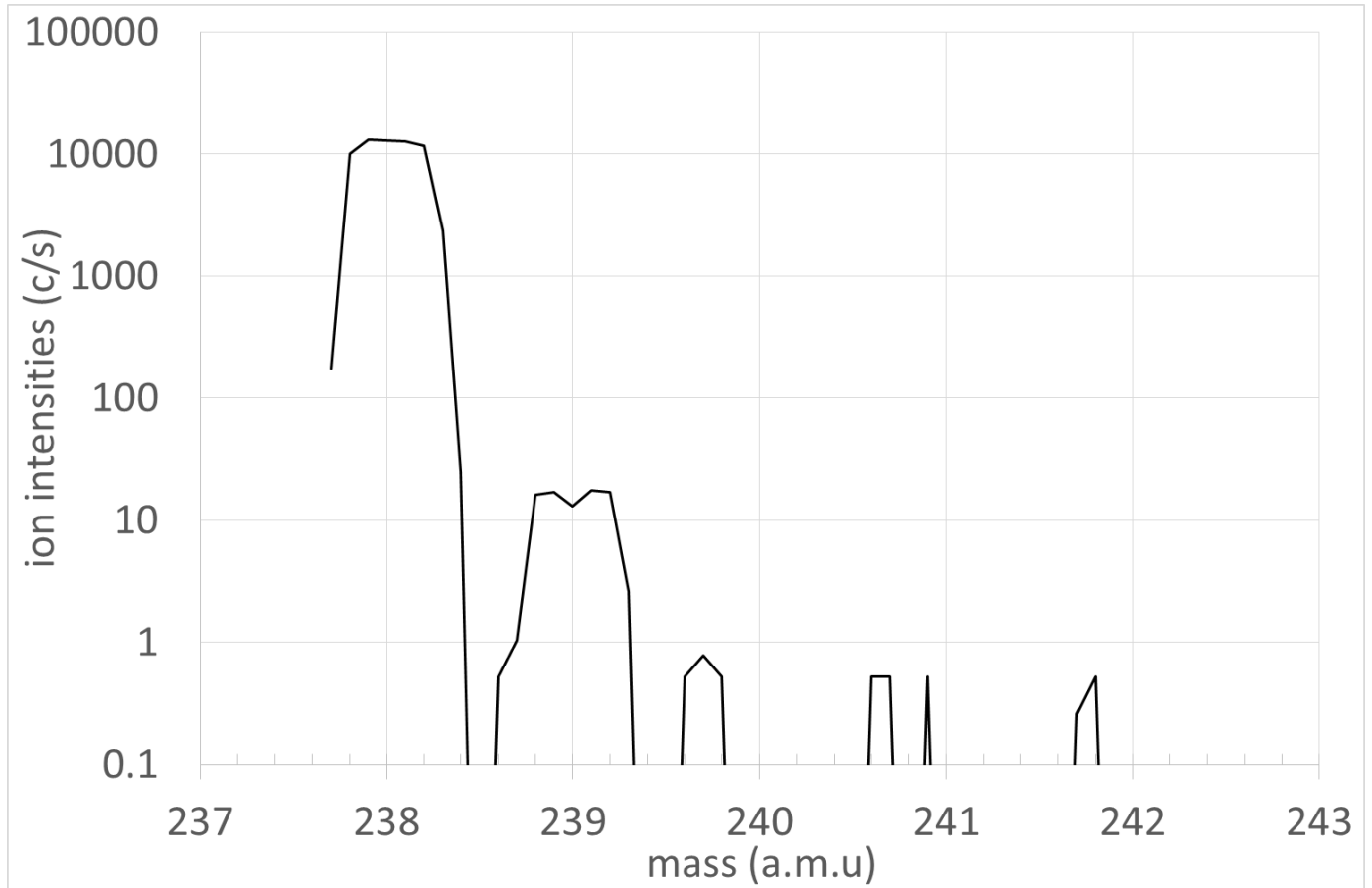
392   the particle (Fig. 9). Unfortunately, the very high uranium hydride formation rate ($^{238}UH^+/^{238}U^+ =$

393   3.10×10^{-3}) did not allow the determination of $^{236}U/^{238}U$ for values lower than 2×10^{-5}, and the

394   ^{236}U concentration was below the limit of detection which is compatible with naturally-

395   occurring uranium with $^{236}U/^{238}U$ isotope ratios ranged from 10^{-15} to 10^{-10} [36, 37]. To measure

396   the ^{236}U at such low levels, other analytical techniques should be performed, such as laser-

397   ablation ICP-MS [12, 38] or Thermal Ionisation Mass Spectrometry (TIMS) [39].

398

399

400   **Fig. 8** ion images at ^{238}U mass obtained with an O_2^+ primary ion current of 250 pA and a raster size of

401   25 µm × 25 µm

402

403

404 **Fig. 9** Mass spectrum on the uranium particle at the plutonium isotope masses, obtained with an O_2^+ primary ion

405 current of 250 pA and a raster size of 25 µm × 25 µm. Intensities at 239 atomic mass units is likely due to $^{238}UH^+$

406 species

407

408 ## Conclusions

409

410 We have developed an analytical methodology to localize and characterize the morphological,

411 elemental and isotopic compositions of α-emitting actinide bearing micro-particles. These

412 analyses were performed on road dust sample collected at 25 km form the FDNPP. Particles

413   containing α-emitting elements were deposited along with numerous mineral matrix particles

414   on polycarbonate plates, embedded in a collodion layer and covered with an SSNTD. Alpha track

415   autoradiography allowed localisation of the active particles. The presence of uranium was

416   confirmedby SEM. Thereafter they were transferred finally to a graphite disk for measurement

417   of isotope composition by SIMS analysis..

418

419   The correlation between the numbers of α-tracks and the mean observed diameters of the

420   corresponding particles measured by SEM led to the rejection of the hypothesis of actinide-

421   bearing particles released during the FDNPP accident. Twenty-eight particles chosen as the

422   strongest α-emitting ones were examined by SEM/EDX, but only four of them were pure

423   uranium particles. Only one of these particles was analysed by SIMS and showed the typical

424   isotopic composition of natural uranium.

425

426   To increase the probability for detection of FDNPP-derived actinide particles, experiments

427   should be performed using larger quantities of samples. In addition, the method for transferring

428   particles from polycarbonate plates to graphite disks for SIMS measurements should be

429   improved. This study however showed that uranium particles can be isolated efficiently from

430   environmental samples and individually analysed by SEM, EDX detector and SIMS. For future

431   analyses, direct isotope analyses could be tested on the polycarbonate plates using laser

432   ablation coupled to ICP-MS. This would avoid the need to dissolve the collodion. as well as the

433   transfer of particles onto another support material. Further measurements will be required on

434   other α-emitting particles detected in soil or road dust samples in order to detect uranium, and

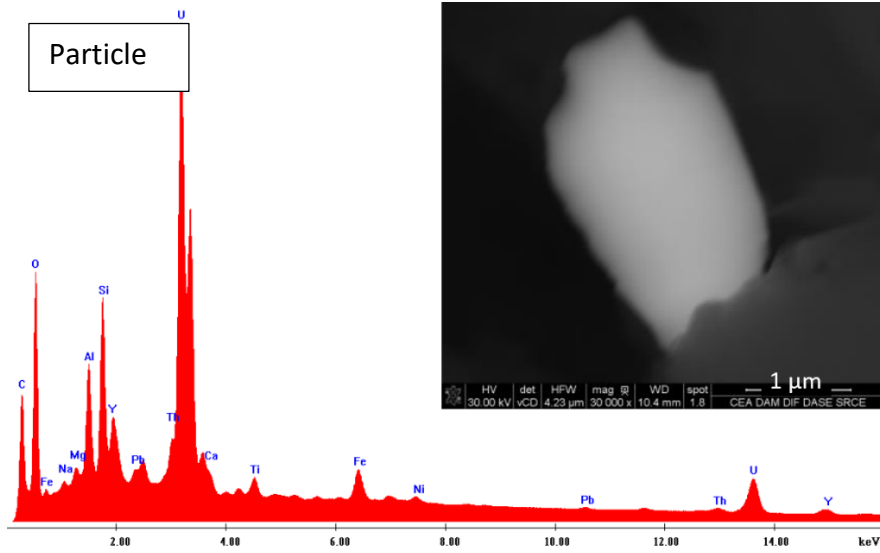435   possibly the plutonium released by the FDNPP.

436

Acknowledgements

References

1. Sakaguchi A, Steier P, Takahashi Y, Yamamoto M (2014) Isotopic compositions of 236U and Pu isotopes in "black substances" collected from roadsides in Fukushima prefecture: Fallout from the Fukushima Dai-Ichi nuclear power plant accident. Environmental Science and Technology 48 (7): 3691–3697. doi: 10.1021/es405294s.

2. Zheng J, Tagami K, Uchida S (2013) Release of plutonium isotopes into the environment from the fukushima daiichi nuclear power plant accident: What is known and what needs to be known. Environmental Science and Technology 47 (17): 9584–9595. doi: 10.1021/es402212v.

3. Evrard O, Pointurier F, Onda Y et al. (2014) Novel insights into fukushima nuclear accident from isotopic evidence of plutonium spread along coastal rivers. Environmental Science and Technology 48 (16): 9334–9340. doi: 10.1021/es501890n.

4. Jaegler H, Pointurier F, Onda Y et al. (2018) Plutonium isotopic signatures in soils and their variation (2011-2014) in sediment transiting a coastal river in the Fukushima Prefecture , Japan. Environmental Pollution 240 167–176. doi: 10.1016/j.envpol.2018.04.094.

5. Schneider S, Bister S, Christl M et al. (2017) Radionuclide pollution inside the Fukushima Daiichi exclusion zone, part 2: Forensic search for the "Forgotten" contaminants Uranium-236 and plutonium. Applied Geochemistry 85 194–200. doi: 10.1016/j.apgeochem.2017.05.022.

6. Shinonaga T, Steier P, Lagos M, Ohkura T (2014) Airborne plutonium and non-natural uranium from the Fukushima DNPP found at 120 km distance a few days after reactor hydrogen explosions. Environmental Science and Technology 48 (7): 3808–3814. doi: 10.1021/es404961w.

7. Yang G, Tazoe H, Yamada M (2016) Determination of ^{236}U in environmental samples by single extraction chromatography coupled to triple-quadrupole inductively coupled plasma-mass spectrometry. Analytica Chimica Acta 944 44–50. doi: 10.1016/j.aca.2016.09.033.

8. Yang G, Tazoe H, Hayano K et al. (2017) Isotopic compositions of ^{236}U, ^{239}Pu, and ^{240}Pu in soil contaminated by the Fukushima Daiichi Nuclear Power Plant accident. Scientific Reports 7 (1): 13619. doi: 10.1038/s41598-017-13998-6.

9. Salbu B (2011) Radionuclides released to the environment following nuclear events. Integrated Environmental Assessment and Management 7 (3): 362–364. doi: 10.1002/ieam.232.

10. López JG, Jiménez-Ramos MC, García-León M, García-Tenorio R (2007) Characterisation of hot particles remaining in soils from Palomares (Spain) using a nuclear microprobe. Nuclear Instruments and Methods in Physics Research Section B: Beam Interactions with Materials and Atoms 260 (1): 343–348. doi: https://doi.org/10.1016/j.nimb.2007.02.044.

11. Lind OC, Salbu B, Janssens K et al. (2007) Characterization of U/Pu particles originating from the nuclear weapon accidents at Palomares, Spain, 1966 and Thule, Greenland, 1968. Science of The Total Environment 376 (1–3): 294–305. doi: 10.1016/J.SCITOTENV.2006.11.050.

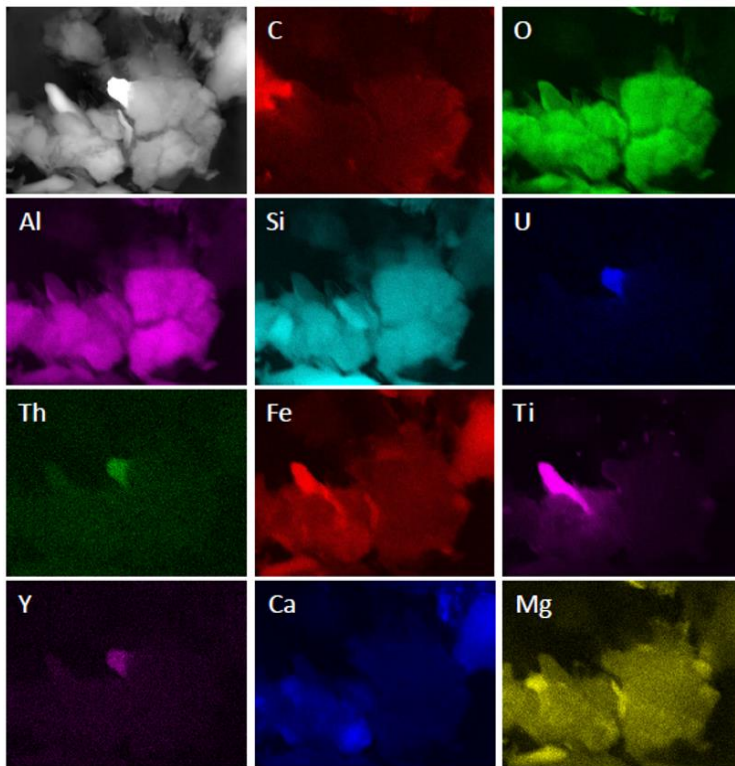12. Boulyga SF, Prohaska T (2008) Determining the isotopic compositions of uranium and

486   fission products in radioactive environmental microsamples using laser ablation ICP-MS
487   with multiple ion counters. Analytical and Bioanalytical Chemistry 390 (2): 531–539. doi:
488   10.1007/s00216-007-1575-6.

489   13.   Ikehara R, Suetake M, Komiya T et al. (2018) Novel Method of Quantifying Radioactive
490   Cesium-Rich Microparticles (CsMPs) in the Environment from the Fukushima Daiichi
491   Nuclear Power Plant. Environmental Science and Technology 52 (11): 6390–6398. doi:
492   10.1021/acs.est.7b06693.

493   14.   Furuki G, Imoto J, Ochiai A et al. (2017) Caesium-rich micro-particles: A window into the
494   meltdown events at the Fukushima Daiichi Nuclear Power Plant. Scientific Reports 7
495   (42731): 1–10. doi: 10.1038/srep42731.

496   15.   Imoto J, Ochiai A, Furuki G et al. (2017) Isotopic signature and nano-texture of cesium-
497   rich micro-particles: Release of uranium and fission products from the Fukushima Daiichi
498   Nuclear Power Plant. Scientific Reports 7 (1): 5409. doi: 10.1038/s41598-017-05910-z.

499   16.   Abe Y, Iizawa Y, Terada Y et al. (2014) Detection of uranium and chemical state analysis of
500   individual radioactive microparticles emitted from the Fukushima nuclear accident using
501   multiple synchrotron radiation X-ray analyses. Analytical Chemistry 86 (17): 8521–8525.
502   doi: 10.1021/ac501998d.

503   17.   Adachi K, Kajino M, Zaizen Y, Igarashi Y (2013) Emission of spherical cesium-bearing
504   particles from an early stage of the Fukushima nuclear accident. Sci Rep. doi:
505   10.1038/srep02554

506   18.   Kaltofen M, Gundersen A (2017) Radioactively-hot particles detected in dusts and soils
507   from Northern Japan by combination of gamma spectrometry, autoradiography, and
508   SEM/EDS analysis and implications in radiation risk assessment. Science of The Total
509   Environment 607–608 1065–1072. doi: https://doi.org/10.1016/j.scitotenv.2017.07.091.

510   19.   Kirchner G, Bossew P, De Cort M (2012) Radioactivity from Fukushima Dai-ichi in air over
511   Europe; part 2: What can it tell us about the accident? Journal of Environmental
512   Radioactivity 114 35–40. doi: 10.1016/j.jenvrad.2011.12.016.

513   20.   Schneider S, Walther C, Bister S et al. (2013) Plutonium release from Fukushima Daiichi
514   fosters the need for more detailed investigations. Sci Rep. doi: 10.1038/srep02988

515   21.   Ochiai A, Imoto J, Suetake M et al. (2018) Uranium dioxides and debris fragments
516   released to the environment with cesium-rich microparticles from the Fukushima Daiichi
517   Nuclear Power Plant. Environ Sci Technol. doi: 10.1021/acs.est.7b06309

518   22.   Yamamoto M, Sakaguchi A, Ochiai S et al. (2014) Isotopic Pu, Am and Cm signatures in
519   environmental samples contaminated by the Fukushima Dai-ichi Nuclear Power Plant
520   accident. Journal of Environmental Radioactivity 132 31–46. doi:
521   10.1016/j.jenvrad.2014.01.013.

522   23.   Yoshida S, Muramatsu Y, Tagami K et al. (2000) Concentrations of uranium and ^{235}U/^{238}U
523   ratios in soil and plant samples collected around the uranium conversion building in the
524   JCO campus. Journal of Environmental Radioactivity 50 (1–2): 161–172. doi:
525   10.1016/S0265-931X(00)00075-8.

526   24.   Yoshida S, Muramatsu Y, Tagami K, Uchida S (1998) Concentrations of lanthanide
527   elements, Th, and U in 77 Japanese surface soils. Environment International 24 (3): 275–
528   286. doi: 10.1016/S0160-4120(98)00006-3.

529   25.   Bu W, Zheng J, Ketterer ME et al. (2017) Development and application of mass

530   spectrometric techniques for ultra-trace determination of [236]U in environmental samples-
531   A review. Analytica Chimica Acta 995 1–20. doi: 10.1016/j.aca.2017.09.029.

532   26.   Esaka F, Magara M (2014) Secondary ion mass spectrometry combined with alpha track
533   detection for isotope abundance ratio analysis of individual uranium-bearing particles.
534   Talanta 120 349–354. doi: 10.1016/j.talanta.2013.12.029.

535   27.   Vlasova IE, Kalmykov SN, Konevnik Y V et al. (2008) Alpha track analysis and fission track
536   analysis for localizing actinide-bearing micro-particles in the Yenisey River bottom
537   sediments. Radiation Measurements 43 S303–S308. doi: 10.1016/j.radmeas.2008.04.029.

538   28.   Zhuk, Lomonosova, Yaroshevich et al. (1995) Investigation of vertical migration of alpha-
539   emitting nuclides in soils for southern regions of the Republic of Belarus. Radiation
540   Measurements 25 (1–4): 385–387.

541   29.   Boulyga SF, Becker JS (2001) Determination of uranium isotopic composition and [236]U
542   content of soil samples and hot particles using inductively coupled plasma mass
543   spectrometry. Analytical Chemistry 370 612–617.

544   30.   Boulyga SF, Desideri D, Meli MA et al. (2003) Plutonium and americium determination in
545   mosses by laser ablation ICP-MS combined with isotope dilution technique. International
546   Journal of Mass Spectrometry 226 (3): 329–339. doi: http://dx.doi.org/10.1016/S1387-
547   3806(03)00024-1.

548   31.   Nishihara K, Iwamoto H, Suyama K (2012) Estimation of fuel compositions in Fukushima-
549   Daiichi nuclear power plant (Date of access: 30/08/2018).

550   32.   Kelley JM, Bond LA, Beasley TM (1999) Global distribution of Pu isotopes and 237Np. In:
551   Sci. Total Environ. pp 483–500.

552   33.   Ellis WR, Wall T (1982) Use of particle track analysis to measure fissile particle size
553   distributions in contaminated soils. Nuclear Instruments and Methods in Physics Research
554   200 (2–3): 411–415. doi: 10.1016/0167-5087(82)90463-X.

555   34.   Fauré AL, Rodriguez C, Marie O et al. (2014) Detection of traces of fluorine in micrometer
556   sized uranium bearing particles using SIMS. Journal of Analytical Atomic Spectrometry 29
557   (1): 145–151. doi: 10.1039/c3ja50245g.

558   35.   Adams JAS, Osmond JK, Rogers JJW (1959) The geochemistry of thorium and uranium. In:
559   Phys. Chem. Earth. pp 298–348.

560   36.   Steier P, Bichler M, Keith Fifield L et al. (2008) Natural and anthropogenic [236]U in
561   environmental samples. Nuclear Instruments and Methods in Physics Research, Section B:
562   Beam Interactions with Materials and Atoms 266 (10): 2246–2250. doi:
563   10.1016/j.nimb.2008.03.002.

564   37.   Sakaguchi A, Kawai K, Steier P et al. (2009) First results on [236]U levels in global fallout.
565   Science of the Total Environment 407 (14): 4238–4242. doi:
566   10.1016/j.scitotenv.2009.01.058.

567   38.   Konegger-Kappel S, Prohaska T (2016) Spatially resolved analysis of plutonium isotopic
568   signatures in environmental particle samples by laser ablation-MC-ICP-MS. Analytical and
569   Bioanalytical Chemistry 408 (2): 431–440. doi: 10.1007/s00216-015-8876-y.

570   39.   Shinonaga T, Donohue D, Aigner H et al. (2012) Production and Characterization of
571   Plutonium Dioxide Particles as a Quality Control Material for Safeguards Purposes.
572   Analytical Chemistry 84 (6): 2638–2646. doi: 10.1021/ac202502z.
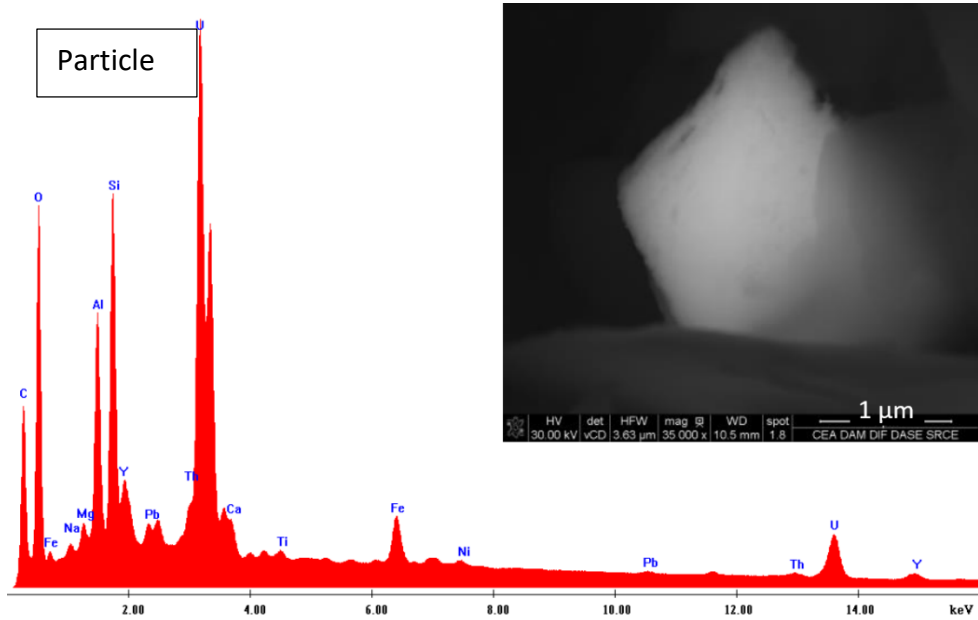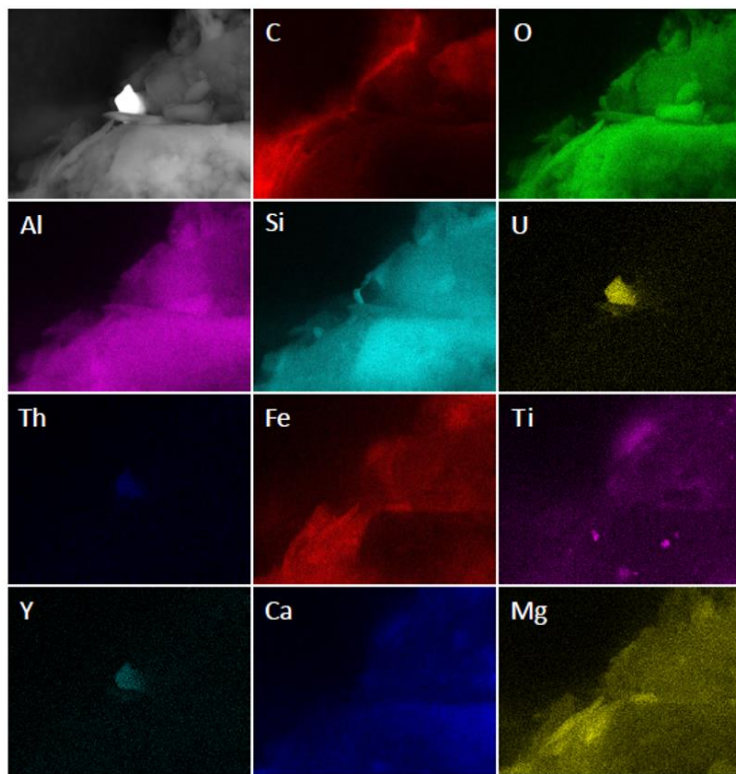
573

574 # Supplementary information

575

576

577 **Fig. S1** Electronic image, EDX spectrum and elemental mapping of the particle #2 identified as an U-bearing

578 particle. The mapping shows qualitatively that some elements (C, O, Al, Si, Fe, Ti, Ca, Mg) detected in the EDX

579 spectrum may come from surrounding particles, whereas Y and Th are obviously present in the particle. This is an

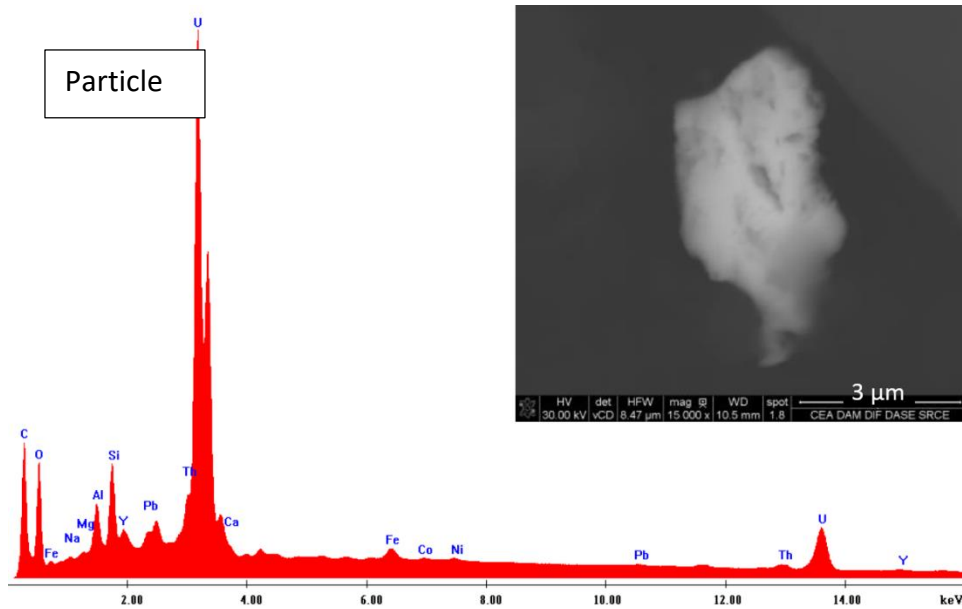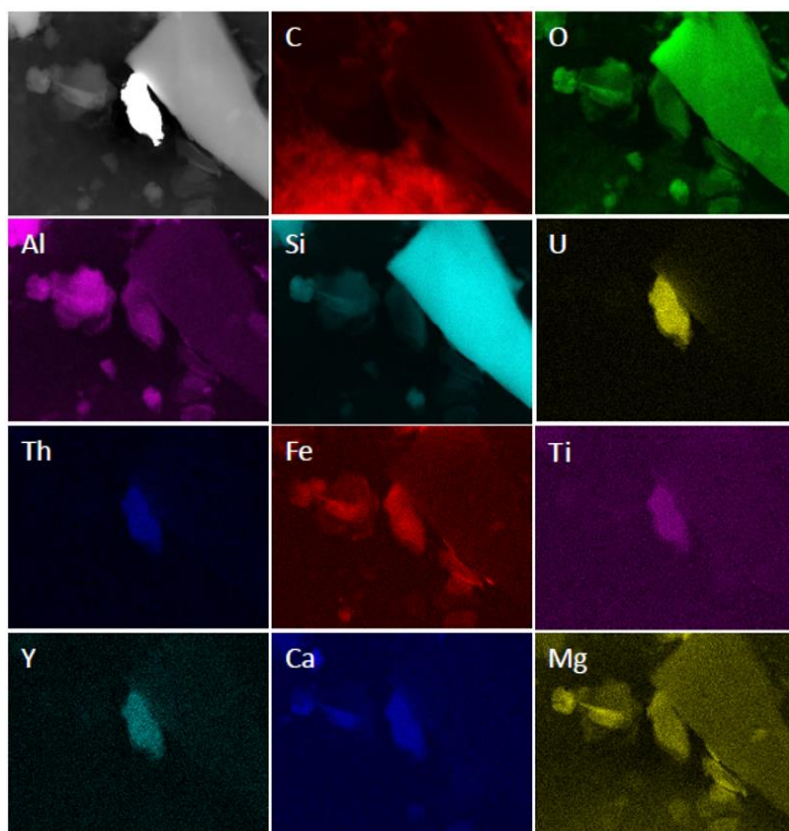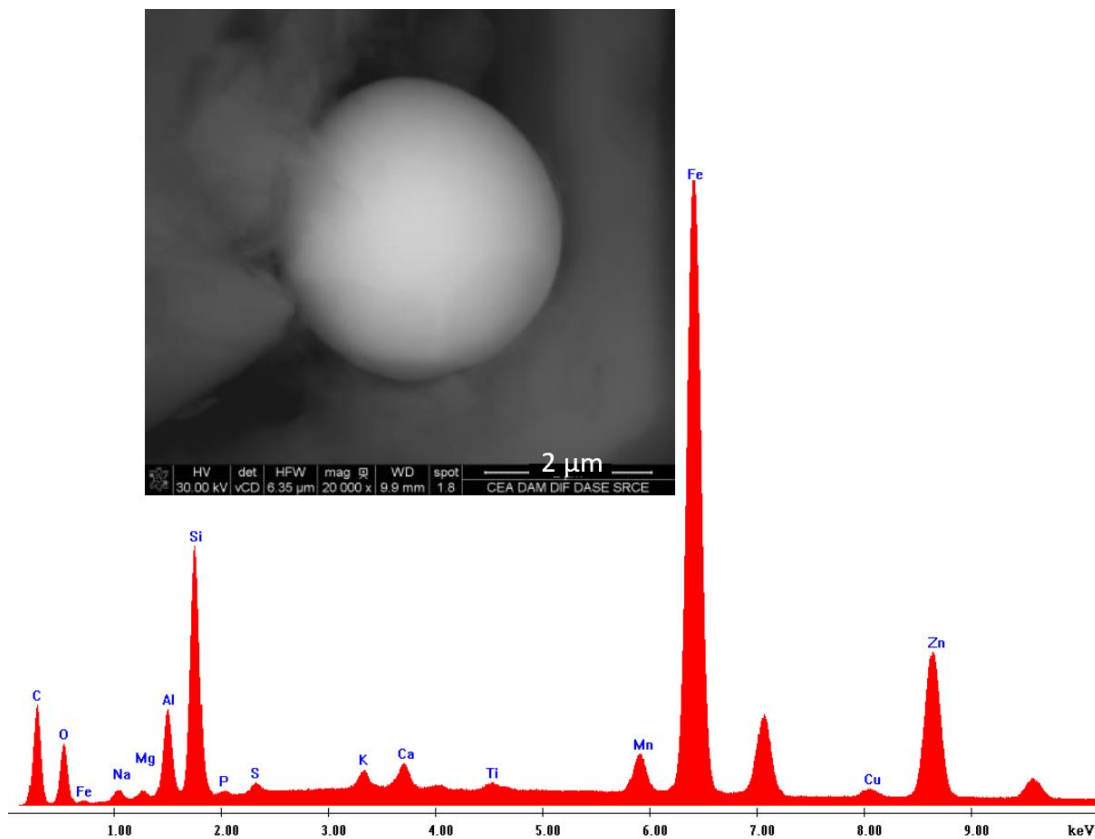580 indication that this U-bearing particule may be of natural origin

581

582

Fig. S2 Electronic image, EDX spectrum and elemental mapping of the particle #3 identified as an U-bearing particle. The mapping shows qualitatively that some elements (C, O, Al, Si, Fe, Ti, Ca, Mg) detected in the EDX spectrum may come from surrounding particles, whereas Y and Th are obviously present in the particle. This is an indication that this U-bearing particule may be of natural origin
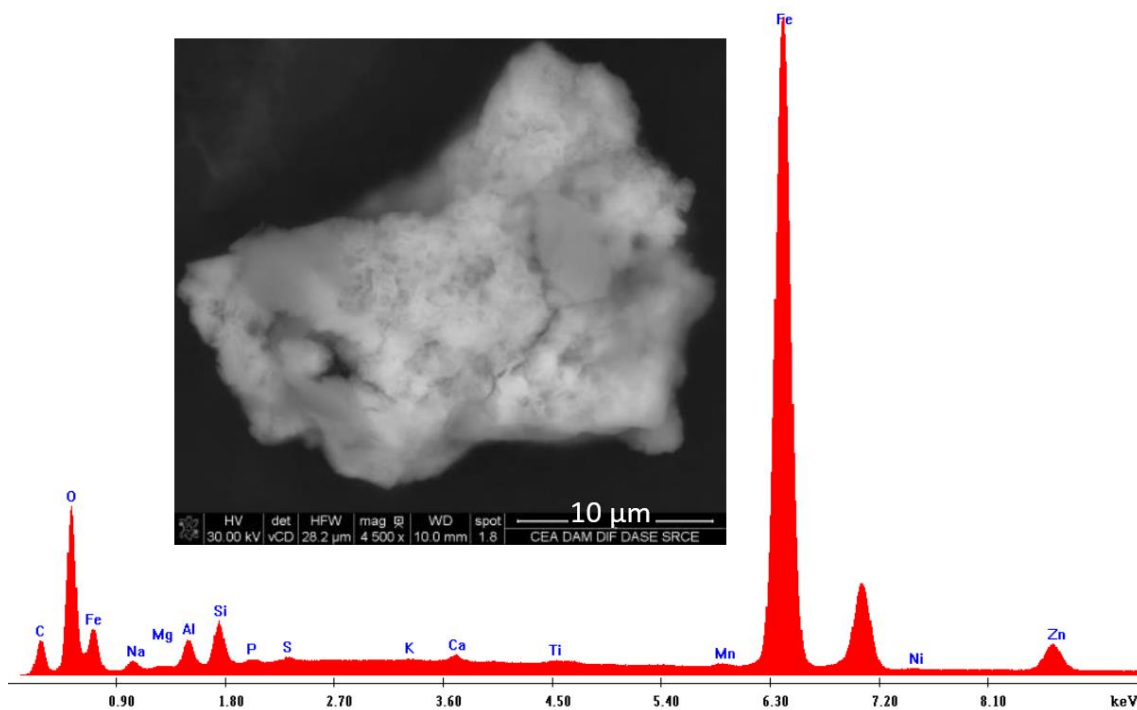
583

584

585

586

587

588

Fig. S3 Electronic image, EDX spectrum and elemental mapping of the particle #3 identified as an U-bearing

particle. The mapping shows qualitatively that all the detected elements detected in the EDX spectrum are

obviously present in the particle. This is a strong indication that this U-bearing particule may be of natural origin
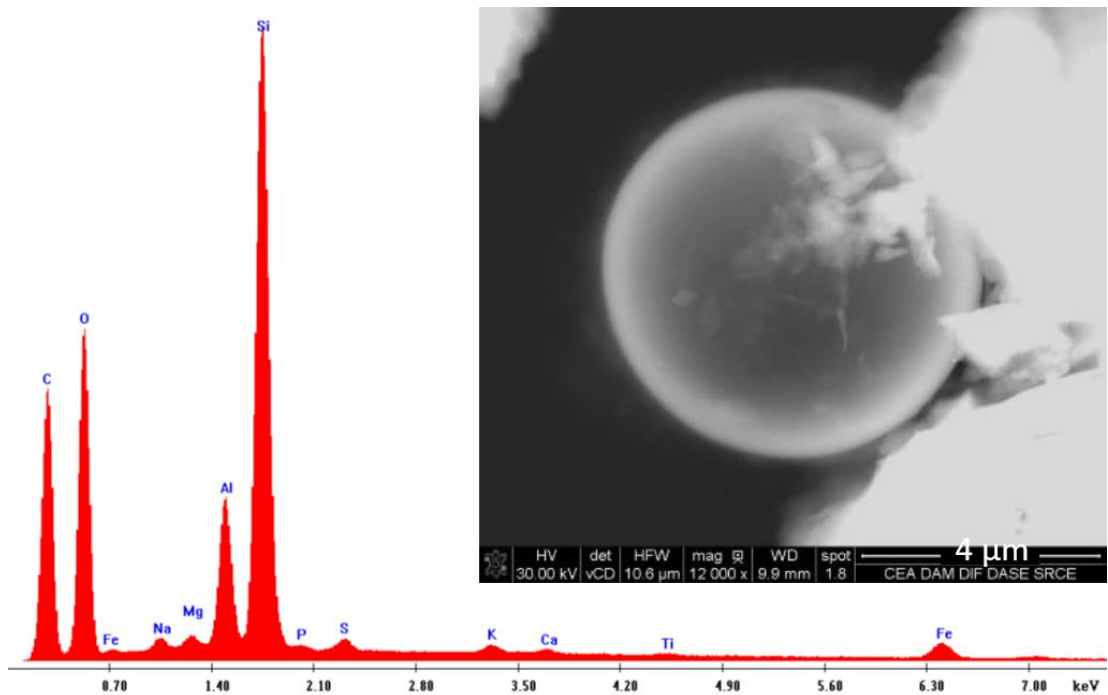
592

593

Fig. S4 Examples of electronic images of FeZn particles and associated EDX spectra

594

595

596   **Fig. S5** Example of an electronic image of a spherical Si particle and associated EDX spectrum.